JOURNAL OF PROPULSION AND POWER
Vol. 13, No. 6, November–December 1997

Velocity and Temperature Measurements in a Low-Power Hydrazine Arcjet

S. A. Bufton* and R. L. Burton†
University of Illinois at Urbana–Champaign, Urbana, Illinois 61801

Recent advances have been made in low-power (1–2 kW) arcjet performance with the aid of numerical, nonequilibrium plasma flow models. Consequently, validation of these models through experimentation has become increasingly important. We discuss diagnostic probe techniques for measuring the exit plane flow of a 1 kW class hydrazine thruster. A spatially resolved time-of-flight electrostatic probe method is described for measurements of radial profiles of the plasma axial velocity u_i. These measurements are combined with previous quadruple probe measurements of T_e and the ion speed ratio u_i/c_m to estimate the ion temperature T_i, resulting in $T_i/T_e \approx T_g/T_e \sim 0.4$ at the thruster exit. The exit plane data for u_i and T_i are compared with computational arcjet model predictions and previous experimental results, showing substantial agreement.

Nomenclature

A_p = probe surface area, m^2
c_m = most probable thermal speed, m/s
d^* = constrictor diameter, mm
f = hydrogen ion fraction n_{H^+}/n_e
I_{arc} = arcjet operating current, A
I_{sat} = ion saturation current, A
k = Boltzmann constant, J/K
m = particle mass, kg
$\dot{m}$ = propellant flow rate, mg/s
n = particle density, cm^{-3}
P = thruster power, kW
r_p = probe radius, mm
T = temperature, K, eV
t = time, μs
u_i = ion axial velocity, m/s
V_{arc} = arcjet operating voltage, V
V_{d2} = electrode relative bias voltage, V
x = axial distance from thruster exit plane, mm
γ = angle of probe to flow velocity, deg
δ = flow divergence angle, deg
θ = angle of probe to axis, deg
λ_D = Debye length, m
λ_{mfp} = collision mean free path, m
ϕ_s = sheath potential at wall, V

Subscripts
e, i, n = electron, ion, neutral species
ex = exhaust
g = gas

Introduction

THE hydrazine arcjet thruster, after 35 years of research and development, has only recently been applied to commercial satellites.[1] Because improved arcjet performance is desired for continued commercial application, detailed diagnostics and accurate numerical models have become increasingly important as design tools. In this paper, we present results for velocity, electron temperature, and heavy particle temperature at the exit plane of a 1-kW hydrazine arcjet. These results give physical insight into arcjet operation and provide data for the validation of arcjet models, used to design arcjets with improved efficiency, specific impulse, and thruster lifetime.

The arcjet used in this study is a 1 kW constricted arc type.[2] The 225:1 nozzle is a 20-deg half-angle cone with a throat (constrictor) diameter d^* = 0.63 mm, and an anode–cathode gap of 0.58 mm. A mixture of 1 mole of nitrogen to 2 moles of hydrogen is used to form simulated hydrazine. This is used for reasons of safety and cost and to allow comparison with previously published results. The hydrazine is delivered to the arcjet from separate flow controllers at a combined rate of 50 mg/s. The arcjet is driven by a power processing unit (PPU) that supplies a nominal 10 A dc current on which a triangular waveform, or ripple, is superimposed. This current ripple produces a corresponding variation in plasma parameters, as detected by oscillations on probe signals in the plume.[3] The arcjet power at 10 A operation is 1.12 kW.

Electrostatic probes have found much use in space and laboratory plasmas. Several researchers have employed classical langmuir[4] single probes in the characterization of low-power arcjet plumes.[5–9] An alternative to the single probe is the triple electrostatic probe,[10–12] which allows simultaneous time-dependent measurement of T_e and n_e at a constant probe bias voltage. A further variation is the quadruple electrostatic probe,[13,14] which combines the triple probe with a crossed probe[15–18] to measure the ion speed ratio u_i/c_m (plasma velocity/ion most probable thermal speed) in flowing plasmas, in addition to T_e and n_e. Flush-mounted single probes are also being used in the arcjet anode to measure current density T_e, n_e, and sheath potential ϕ_s at the nozzle wall.[19]

Velocity and Temperature Measurements

While several researchers have performed velocity and temperature measurements on low-power arcjets operating with ammonia and hydrogen propellants, few studies have investigated hydrazine. The research by Zube and Myers[20] remains the only comprehensive internal nozzle study of the state of the plasma in a low-power hydrazine arcjet, employing emission spectroscopy techniques inside a 1-kW arcjet nozzle. Their results implied that thermal kinetic nonequilibrium was significant between the heavy particles and the electrons. They

Presented as Paper 95-3066 at the AIAA/ASME/SAE/ASEE 31st Joint Propulsion Conference, San Diego, CA, July 10–12, 1995; received Feb. 2, 1996; revision received June 24, 1997; accepted for publication June 30, 1997.

*Graduate Student, Department of Mechanical and Industrial Engineering. Student Member AIAA.

†Professor, Department of Aeronautical and Astronautical Engineering, 104 S. Wright Street, Urbana, IL 61801. Associate Fellow AIAA.

also noted excitational, rotational, and vibrational nonequilibrium among the heavy particle species.

Emission spectroscopy has also been applied to the interior nozzle region of a 26-kW class ammonia thruster[21] and to arcjet plumes.[22–26] The laser induced fluorescence (LIF) technique has been used successfully to measure heavy particle temperatures and exit plane velocity profiles in ammonia[27–29] and hydrogen[29–33] arcjets. Results showed velocity slip between the N and H species, with the atomic nitrogen axial velocity ~9% larger than that of atomic hydrogen.

These results contrast those of Liebeskind et al.,[29] who investigated velocity slip in a 1-kW helium-seeded hydrogen arcjet via LIF measurements. The upper limit of the slip between the two probed species was ~2%, which was also the uncertainty of the velocity measurements. They also noted that the measured kinetic temperatures of H and He agreed to within 6%.

Finally, a velocity measurement technique called current modulation velocimetry (CMV) was developed and implemented on a 1-kW hydrogen arcjet,[34,35] from which the time-of-flight (TOF) electrostatic probe technique employed in the present study is derived. In this technique, a short-duration current pulse is superimposed on the arcjet steady-state operating current, causing a momentary change in the emission characteristics of the tagged flow, which is monitored optically at two axial locations in the plume. The plasma velocity is inferred by measuring the time required for tagged plasma to traverse the axial distance between detectors. This technique followed from the emission ripple velocimetry (ERV) technique developed by Spores et al.,[36] in which plasma velocities were inferred by monitoring natural fluctuations in the plasma emission.

Velocities have been measured elsewhere in electric propulsion devices using TOF electrostatic double probes.[25,37,38] For the TOF technique used in the present study, a double-probe configuration is not used because of the size constraints placed on the TOF probe by the small volume of the plasma to be probed.

Power Processing Unit

Periodic oscillations or ripple generated by the PPU cause fluctuations in the signals of the two TOF electrodes. However, these fluctuations are difficult to interpret for velocity measurements because the expected time delay between the TOF signals (~1 μs) is much smaller than the 53-μs period of the PPU-supplied current ripple. By artificially imposing a narrow pulse on the arcjet current, which causes a short-duration fluctuation, the resolution of the TOF technique can be greatly improved over one using PPU ripple. That is, the temporal location of a fast fluctuation is more easily discerned than that of a much longer (53-μs) effect.

TOF Velocimetry Diagnostic

The TOF technique, used here for measuring spatially resolved velocities in the arcjet plume, uses a short-duration current-deficit pulse superimposed on the arcjet current to produce a local electron saturation current minimum, which is detected by a miniature electrostatic TOF probe. The probe provides a spatial resolution of 5 mm, eliminating the need to Abel-invert the data as required by line-of-sight optical methods. Figure 1 shows the TOF probe, which consists of two 0.75-mm-diam tungsten wires, electrically insulated along most of their length by two 1.6-mm o.d. alumina tubes. The exposed length of each tungsten electrode is 0.25 mm, the exposed area is 1.03 mm^2, and the axial separation between the two electrodes is 5.0 mm (±2%). The elevation of the probe is such that the arcjet thrust axis is centered between the two sensing electrodes. The TOF electrodes are biased 24 V above the grounded arcjet anode to monitor the local electron saturation current density at each measurement location. The probe responds to variations in the probe saturation currents as the plasma convects over the two

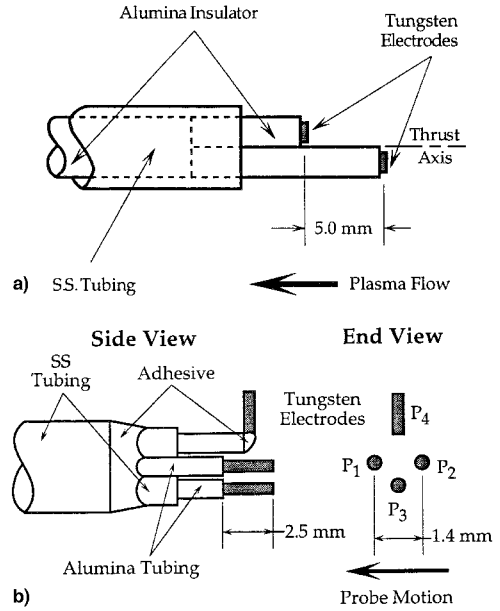

Fig. 1 Schematic views of the a) TOF electrostatic probe and b) quadruple probe (Ref. 14).

TOF electrodes, with the flow velocity determined by the temporal separation of these signals and the electrode separation.

No effort was made to clean the probe by electron or ion bombardment. Although langmuir probe contamination can have a marked effect on T_e measurements,[10,13] the TOF probe detects the arrival time of plasma density fluctuations rather than T_e variations and, therefore, is relatively insensitive to contamination.

Probe Length Scales

For conditions expected at the exit plane probe location (T_e ~ 0.6 eV, $n_e \sim 4 \times 10^{12}$ cm^{-3}),[14] the Debye length is 3×10^{-4} cm and the ratio of electrode radius to Debye length is $r_p/\lambda_D = 125$. For the probe located 5 mm downstream, this ratio increases to $r_p/\lambda_D \sim 150$. Thus, the sheath surrounding the electrodes can be classified as thin. Although the probe is physically intrusive, the probe electrodes (0.75 mm diameter) are in the near-free molecular flow regime ($\lambda_{mfp} > r_p$). The ratio of the nozzle exit plane area to probe frontal area is 160, and probe blockage is expected to be acceptably small.[3] Furthermore, probe–plasma collisional perturbations are expected to be similar at each electrode, thereby having a minimal effect on the differential convective time delay.

The TOF probe is accurately positioned and repeatably swept through the thruster plume with the probe mount system shown in Fig. 2. The complete assembly is fastened to a stepper motor mounted on a linear translation carriage.[14] The motor and probe assembly carriage are capable of ±5 cm linear translation perpendicular to the arcjet axis, allowing the probe to be manually swept through the plume at ~20 cm/s. Carriage and probe position are determined to 0.25 mm during the TOF pulse by a precision fast response 10-kΩ linear potentiometer (Fig. 3) coupled to the carriage manual drive shaft. Probe position is determined by calibrating the potentiometer output against the o.d. of the anode. The probe support arm is coupled directly to the step motor shaft with the probe tip on the shaft axis (Fig. 2), allowing the probe angle to be varied in 0.9-deg increments without changing the probe tip location.

Probe elevation is repeatably located to within 0.5 mm by aligning the probe center with a line etched on the arcjet anode. The separation between the probe tip and the thruster exit plane is reliably set with 0.1 mm accuracy with a spark gap gauge. For a 1.0-mm probe-to-nozzle spacing, the gap is set at 1.7 mm, because the arcjet mount deflects into the tank 0.7 mm when applying vacuum, introducing a systematic error that

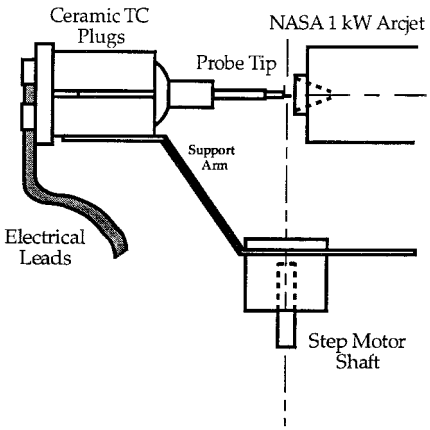

Fig. 2 Schematic of the probe mount. The step motor can be rotated in 0.9-deg increments to align the probe axis with the velocity vector, and the entire assembly can be translated perpendicular to the thrust axis to sweep across the nozzle exit plane.

does not affect the relative spacing of subsequent axial probe positions.

Current Deficit Circuitry

The circuit used to modify the arc current (Fig. 3) is similar to that used in previous CMV studies.[34,35] The current pulse is initiated by closing, for a few microseconds, a switch to a 1-μs time constant resistor–capacitor (R–C) circuit in parallel with the arcjet, causing a sudden decrease in arc current while the capacitor charges. The R–C element used in this study consists of a 0.1-μf capacitor in parallel with a 1-MΩ resistor, both of which are in series with a 10-Ω resistor. Originally, the R–C circuit element was represented by a single resistor (20–30 Ω), but ringing on the edges of the resulting square current pulse obscured the desired TOF probe signals. Switch closure is accomplished with a field-effect transistor (FET), which is closed by the gate pulse as shown in Fig. 3. The resulting short-duration current deficit results in a tagging of the arcjet plasma, primarily in the arc constrictor region.

Because the gate pulse must be positive relative to the FET voltage, and the arcjet cathode and FET operate at ~−100 V below ground, the FET driver circuit (Fig. 3) is a necessary buffer between the FET and the Hewlett-Packard (HP) pulse generator. Because the probe is swept relatively slowly (20 cm/s), the probe location is effectively frozen during the ~3–4 μs elapsed time between the initial trigger and the monitoring of the tagged plasma at the TOF electrodes.

The effect of the current-deficit pulse on thruster operation is shown in Fig. 4, which displays the arcjet current I_{arc} and voltage V_{arc} vs time during a typical pulse. The effect of the pulse on V_{arc} and the magnitude of the current ripple are also evident. The current drops suddenly when the FET switch closes and the 0.1-μF capacitor begins to charge. After a few microseconds, the current through the FET leg of the circuit decreases, and the arc current resumes its normal waveform after a small positive overshoot. The width of the current-deficit pulse is ~4 μs.

The response of V_{arc} (Fig. 4) is to overshoot by ~20 V at the end of the current-deficit pulse. There are several explanations for this behavior. First, the derivative of the arc current (dI_{arc}/dt) has the same qualitative behavior as V_{arc} during the current-deficit pulse, suggesting an inductive voltage drop. Second, the arc has cooled down during the deficit pulse, temporarily increasing the plasma resistivity, and the voltage overshoots until the plasma can recover its original prepulse temperature. Third, the overshoot may be generated by capacitor ringing.

To trigger the current-deficit pulse accurately at each desired radial location, use is made of the voltage output of the precision linear potentiometer, which is mechanically connected

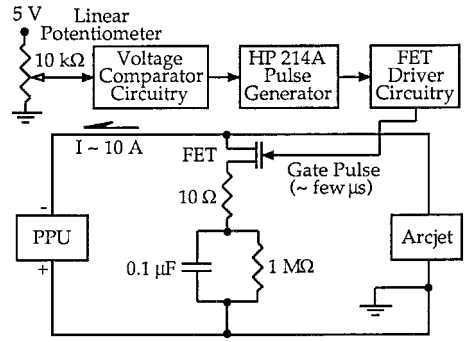

Fig. 3 Schematic of circuit used to trigger the arcjet current-deficit pulse for TOF velocimetry. Momentarily closing the FET switch diverts PPU current away from the arcjet.

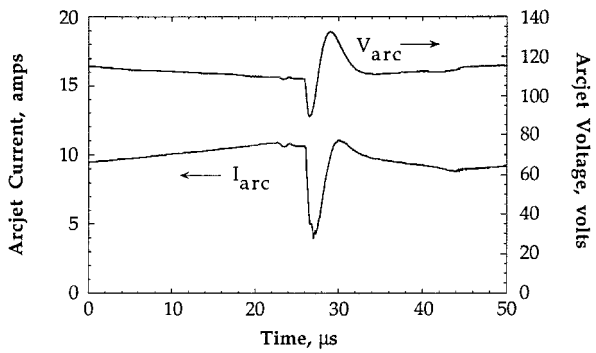

Fig. 4 Variation of I_{arc} and V_{arc} during the current-deficit pulse. The pulse width is much smaller than the period of the PPU ripple.

to the translating probe mount. The voltage of the desired measurement location is set at the voltage comparator circuit (Fig. 3), which generates a single trigger signal to the HP 214A pulse generator as the probe passes the desired radial position.

Effect of Current Ripple

The response of electrostatic probes at the exit plane is determined by the local time-dependent values of n_e and T_e, which oscillate with the PPU-induced current ripple. Figure 5 shows a quadruple probe measurement of centerline ion saturation current density $j_3 \sim I_{sat}/A_p$, plotted with I_{arc} vs time.[14] The probe current is in phase with the arc current, except for a delay of ~3–4 μs associated with the plasma convection time from the arc-heating region near the constrictor to the probe. Accounting for differences in average velocity and measurement location, this delay for hydrazine is consistent with previous triple probe results for the hydrogen arcjet.[34]

The time variation of T_e and n_e on centerline because of current ripple is detected by the signal response of a quadruple probe[14] (Fig. 6). The upper curve, labeled V_{d2}, is the voltage difference between two electrodes of the quadruple probe and varies linearly with T_e for $V_{d2} < 1.5$ V. As current increases from 9.2 to 10.8 A, the V_{d2} signal indicates that T_e decreases 10% from 7300 to 6600 K. The lower curve is the electron saturation current and varies as $n_e(T_e)^{1/2}$, or approximately as n_e. This current closely follows the phase of the PPU current ripple (Fig. 5), indicating that while T_e is decreasing, n_e increases ~40% from a level of $\sim 3 \times 10^{12}$ cm^{-3}. Thus, Figs. 5 and 6 indicate that the n_e variation is in phase with the current ripple and T_e is 180 deg out of phase. Note that T_e is in phase with the ripple of V_{arc}, which is out of phase with I_{arc} because of the negative impedance characteristic of the arcjet. Thus, T_e varies in phase with the local plasma electric field.

Unexpectedly, these results are reversed in phase from those measured previously on a hydrogen arcjet with current ripple,[33] for which n_e decreased and T_e increased with increasing I_{arc}. It

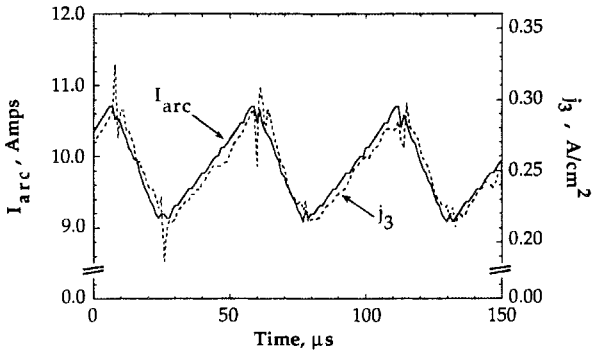

Fig. 5 Arcjet current I_{arc} and ion saturation current density j_3 showing the effects of the PPU ripple. The delay between I_{arc} and j_3 is ~3–4 μs.

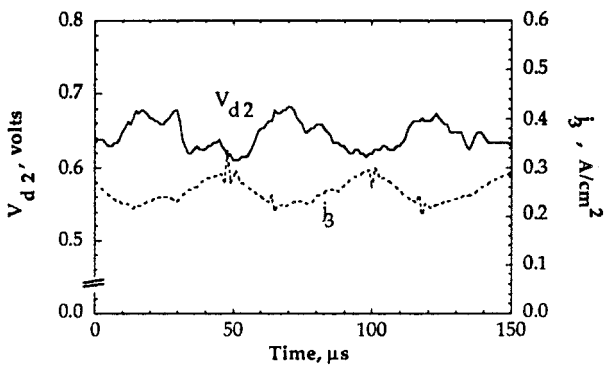

Fig. 6 Variation of T_e and n_e with time, caused by input current ripple. The voltage V_{d2} is proportional to T_e, and current j_3 is proportional to $n_e(T_e)^{1/2} \approx n_e$. Comparison with Fig. 5, on the same time-base, shows that n_e increases and T_e decreases with increases in the arcjet current.

is unclear at this time if this is an indication of a fundamental difference in the operating physics of the hydrazine and hydrogen arcjets. On a steady current basis, increasing the arc current decreases arc resistance, suggesting an in-phase relationship for T_e assuming predominantly coulomb collisions. The reverse results for hydrogen are real, but not explained. It is clear, however, that the T_e and n_e ripples are 180 deg out of phase.

Because of the ripple-induced variation in T_e and n_e, mean values of quadruple probe currents and voltages are used to determine the mean values of T_e, n_e, and $u_i/c_{m,H^+}$. This is achieved by applying a moving average smoothing routine to the raw data.

Experimental Velocity Results and Analysis

Electrostatic TOF probe experiments were carried out in a 1.5-m^3 tank at ~200 mtorr ambient pressure. Measurements were made at the thruster exit plane at a flow rate of 50 mg/s of $2H_2 + N_2$ to simulate fully decomposed hydrazine, at 10.0 A and 112 V, giving $P/\dot{m}$ = 22 MJ/kg, in the middle of the operating range for this arcjet.[2] Anode temperatures were monitored with an optical pyrometer to determine the onset of steady-state operation.

Probe radial surveys of velocity were performed in the arcjet near-field plume, with the probe tip located 1.0 mm from the exit plane. For each data point, the probe carriage and probe were swept manually across the exit plane, generating a signal on the linear potentiometer. The arcjet current-deficit pulse was triggered from this at the same phase in the PPU current ripple (Fig. 4), just after peak current, producing a convected wave of low n_e, which passed the staggered probe tips sequentially (Fig. 1).

The TOF probe response, recorded digitally at 125 MHz, is shown in Fig. 7 for a typical centerline axial velocity measurement. The signal measured at the downstream electrode has been increased by a factor of 6 to account for the lower electron saturation current (lower T_e and n_e) at that location. Both the upstream and downstream electrodes show noise beginning at $t \sim 2$ μs corresponding to the closing of the FET switch. Approximately 3 μs later, the effect of the arcjet current pulse is monitored as a decrease in the electron current to the upstream electrode. After a <1 μs time delay for the tagged flow to traverse the 5-mm electrode separation, a similar decrease is noted at the downstream electrode. For both signals, the width of the deficit in the electron current is ~4 μs, approximately the same as that of the arcjet current deficit pulse. The convective time delay is derived from the probe response (Fig. 7) using the time delay between electron saturation current minima, determined from the zero crossings of the time derivative of the smoothed probe signal (Fig. 8).

Electron saturation current depends primarily on n_e in this regime, because the thermal speed varies less than 10% with variations in T_e. Because the plasma is neutral on the millimeter length scale of the probe separation ($\lambda_D \sim 10^{-6}$ m), the electron density deficit corresponds to an ion density deficit, and the probe measures the ion convective velocity. This velocity is also the neutral velocity, to the extent that the velocity slip between ions and neutrals is small. This is believed to be the case here, as indicated by LIF measurements[27,28] and calculations of the heavy particle mean free path.

Results of TOF probe centerline velocity measurements are shown in Fig. 9 for three separate cold-start sequences. The data show that the centerline axial velocity initially averages ~6.0 km/s during thruster warm-up. After approximately 5–7 min of run time, the axial velocity averages ~6.5 km/s. These cold-start data are consistent with previous results, which indicate that exit plane n_e measurements reach steady

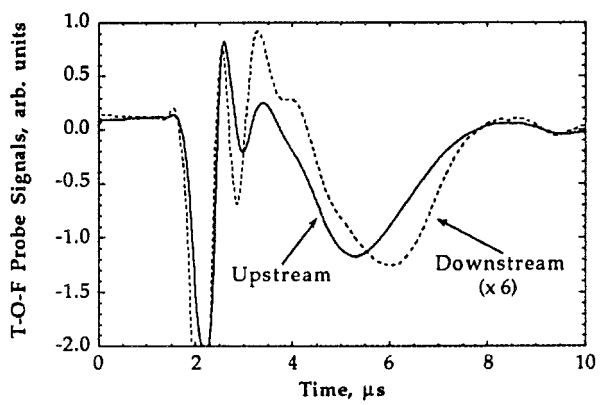

Fig. 7 Variation of the TOF probe signals during a typical current-deficit pulse. The probe electrode signal delay is ~0.77 μs (see Fig. 8).

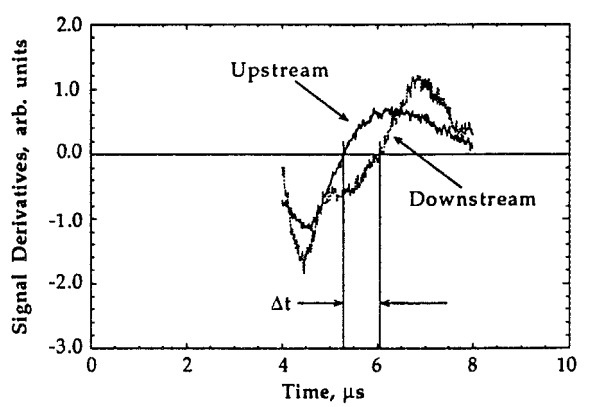

Fig. 8 Derivatives of the smoothed TOF probe signals (Fig. 7) depicting zero crossings at signal minima locations.

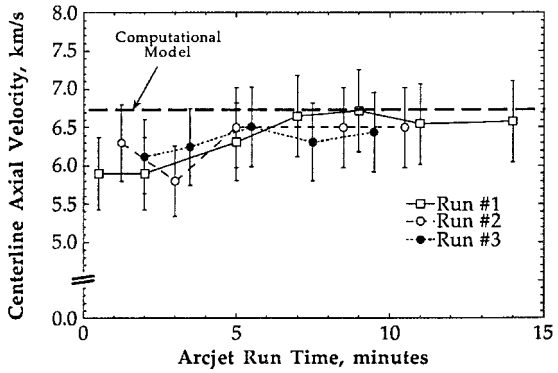

Fig. 9 Measured centerline axial velocity vs time for arcjet warm-up. The numerical model prediction is also shown.

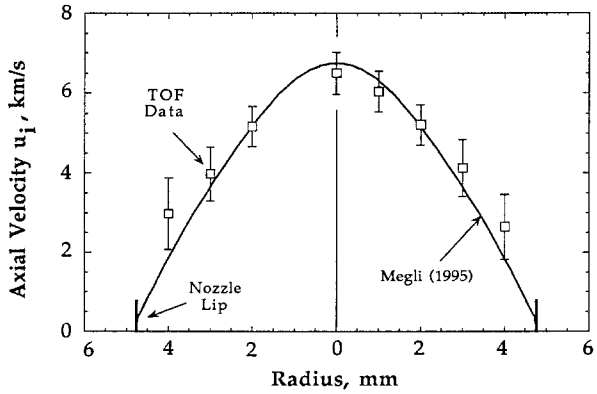

Fig. 10 Experimental measurements and numerical model predictions[39] of the plasma axial velocity profile at the thruster exit.

state after 4–8 min.[39] During the warm-up period, measured velocities appear to vary between 5.8 and 6.3 km/s, although these variations are smaller than the experimental uncertainty, which is discussed later in this paper. Similarly, steady-state centerline axial velocities vary from 6.3 to 6.7 km/s. In previous work,[33] utilizing CMV for a 1-kW hydrogen arcjet, similar velocity fluctuations were observed, and it was determined that the phase of the PPU ripple was not responsible. It is unclear what may be causing the variation in the present measurements.

The TOF probe was swept in radius to generate a radial profile of axial velocity at the thruster exit plane. It was found that using a fixed probe angle ($\theta = 0$ deg) produced a flat or even inverted profile with a velocity minimum on the centerline, caused by misalignment of the probe with δ. An off-axis misaligned TOF probe ($\theta < \delta$) will have its downstream electrode located on a faster velocity streamline. Additionally, the electrode separation along the streamline is less than the geometric separation (5.0 mm) by the factor $\cos(\delta - \theta)$. Both of these factors artificially increase the measured axial velocity, with the former having a greater effect than the latter.

Although the plasma streamlines are not known a priori, the error associated with TOF probe misalignment for off-axis measurements is reduced by aligning the probe with the expected flow vector. The flow divergence has previously been measured 10 mm downstream from the thruster exit[5] and is expected to be larger than the flow streamline angle inside the nozzle at the TOF probe location. For TOF measurements at $r = 0$, 1, 2, 3, and 4 mm, the probe angles were set at $\theta = 0$, 10.8, 18.0, 25.2, and 45.0 deg, respectively. The velocity V measured in this manner is the component along the probe axis and is related to the axial component by $u = V \cos\theta$.

Uncertainty in Axial Velocity Measurement

The experimental uncertainty in the TOF measurement of the axial velocity has four sources: 1) the TOF electrode axial separation; 2) the temporal resolution of the digitizing recording oscilloscope; 3) determination of the time delay of the TOF signals; and 4) probe misalignment with the plasma flow. Because interpretation of the TOF signal magnitudes is not a prerequisite for determining the convective time delay, there are no uncertainties associated with either the method of measuring the collected current or theories governing the charged particle collection. The magnitudes of these uncertainties are summarized next.

1) The 5-mm spatial separation of the TOF electrodes was repeatably measured with calipers to be 5.0 ± 0.1 mm, giving a corresponding uncertainty in the velocity results of ±2%.

2) The TOF electrode signals were sampled with an HP 54510A scope at a sampling rate of 125 MHz. Based on a convective time delay of 1 μs, this results in a 1% uncertainty as a result of the resolution of the oscilloscope.

3) The method used to discern the convective time delay between the two TOF signals is estimated to be accurate to within ±10 sampling intervals, or ~0.08 μs. Based on the measured time delays on the order of 1 μs, this leads to an ±8% uncertainty.

4) Because the plasma streamlines are not known a priori, there is an additional uncertainty associated with misalignment between the TOF probe axis and the flow divergence angle. This uncertainty relates only to the off-centerline measurement locations, as the flow divergence on the thruster centerline is close to 0 deg because of the symmetry of the arcjet. An upper limit can be placed on the magnitude of the associated error by considering realistic limits of the misalignment for each radial measurement location.

For locations near the thruster axis where the flow divergence is expected to be slight, the uncertainty is small as well, because the error ~ $\cos\gamma$, where $\gamma = \delta - \theta$ is the difference between the assumed flow divergence and the actual direction of the flow. For locations far from the centerline (i.e., $r = 3$ and 4 mm), the uncertainty in the flow divergence angle is much larger, and uncertainty in the axial velocity is larger as well. Additionally, for probe misalignments greater than ~10 deg, the width of the probe seen by the plasma becomes a significant percentage of the thruster diameter, and the spatial resolution of the probe is compromised. Based on these arguments, the additional uncertainties in the axial velocity measurements caused by TOF probe misalignment are estimated to be ±0, ±2, ±5, ±15, and ±30% for measurements made at radial locations of 0, 1, 2, 3, and 4 mm, respectively. Combining these uncertainties, the rms uncertainties in the axial velocity measurements are ±8.3, ±8.5, ±10, ±17, and ±31% for measurements made at $r = 0$, 1, 2, 3, and 4 mm, respectively.

Figure 10 shows the resulting symmetric profile of axial velocity measurements made at the thruster exit plane, with the tip of the upstream electrode located 1.0 mm from the exit, and probe midpoint at $x = 2.2$ mm. Also plotted is the profile predicted by a computational model, as discussed next.

Derivation of Heavy Particle Temperature

In a previous study,[14] the ion speed ratio u_i/c_m, where $c_m = (2kT_i/m_i)^{1/2}$, was determined for the same arcjet conditions. Combining the u_i measurements in this paper with those of the ion speed ratio we can determine the quantity $(2kT_i/m_{H^+})^{1/2}$ and, hence, the ion temperature.

Uncertainties in the quadruple probe measurement of the ion speed ratio $u_i/c_{m,H^+}$ as a result of plasma composition,[14] from uncertainties associated with the crossed probe theory,[15,17] and from uncertainties associated with the probe area,[14] result in an overall rms uncertainty of ±15%. Combining the centerline uncertainties in $u_i/c_{m,H^+}$ (±15%) and u_i (±10%) corresponds to an uncertainty in c_{m,H^+} of ±20%. The mean free path for heavy particle collisions (ion–atom, atom–molecule, etc.) at the exit plane is 0.2–0.4 mm, a fraction of the electrode separation distance, allowing the assumption of an equilibrium transla-

tional temperature among these particles; i.e., $T_g \approx T_i$. From the dependence of $T_g \approx T_i$ on $(c_{m,H^+})^2$, this corresponds to an uncertainty in T_g of $\pm 45\%/-35\%$ on the centerline.

A correction to T_g is created both by the T_g radial profile and by the off-axis position of the perpendicular quadruple probe electrode P_4, because P_4 collects ion current I_4 based on the distribution of u_i and T_i along its 2 mm length. For a probe on the centerline, the electrode current I_4 is understated because of the profile decrease in ion density and u_i at the off-centerline position of P_4. Conversely, because I_4 is proportional to $(T_i)^{-1/2}$, a T_i profile with a maximum at the centerline tends to overstate the measured ion current at P_4. Estimating a net 10% understatement of I_4 caused by the off-axis position of P_4 increases the ratio $u_i/c_{m,H^+}$ by 20%, and the value of T_g is reduced by 30%. This is combined with the centerline uncertainty for an overall uncertainty of $+5\%/-50\%$ (Fig. 11), and in the data point at 2 mm (Fig. 12).

At a location $x = 2.2$ mm, the quadruple probe yields a value of $u_i/c_{m,H^+} = 1.00 \pm 15\%$, so that the most probable speed for H^+ is approximately equal to the directed ion velocity.[14] For the measured centerline velocity $u_i = 6.5$ km/s, the heavy particle temperature is then $T_g \approx T_i \approx 3000$ K. With previous results for $T_e \sim 7000$ (Ref. 14), the degree of thermal nonequilibrium on-axis at the thruster exit is indicated by $T_g/T_e \sim 0.4$. In comparison, Zube and Myers,[20] using a similar hydrazine arcjet, spectroscopically measured $T_{exc} \sim 9000$ K and $T_{N_2,vib} \sim 2500$ K at an area ratio of 127, indicating a somewhat higher degree of nonequilibrium than shown here.

Although axial velocity measurements for hydrazine arcjets have not been previously published, the results presented here can be roughly compared with exit plane velocities for 1-kW arcjets operating on other propellants. Arcjets operating on hydrogen at 950 s specific impulse (average exhaust velocity $u_{ex} = 9.3$ km/s), have centerline velocities at the thruster exit of $u_i \sim 14$ km/s (Ref. 30), or $u_i/u_{ex} = 1.5$. In comparison, for this hydrazine arcjet at 420 s ($u_{ex} = 4.1$ km/s) and $u_i = 6.5$ km/s, $u_i/u_{ex} = 1.6$. The measured velocity is therefore close to the value expected, based on a specific impulse argument.

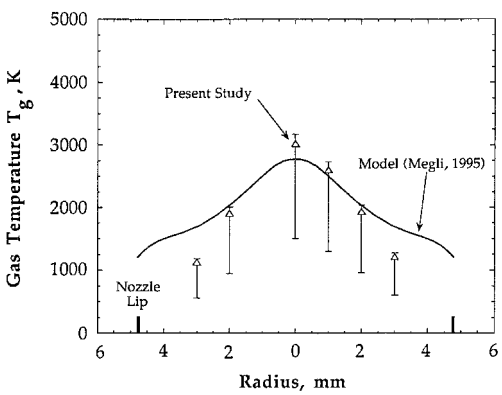

Fig. 11 Experimental measurements and numerical model predictions[39] of T_g profile at the thruster exit.

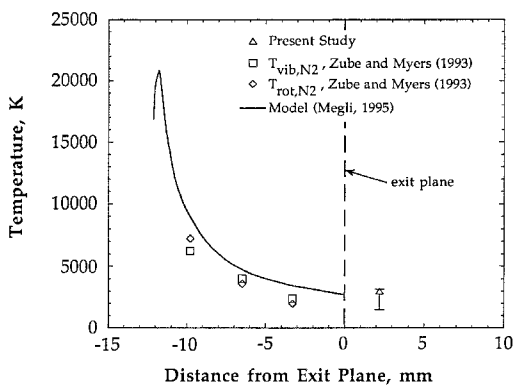

Fig. 12 Comparison of exit plane centerline gas temperature measurements with numerical model predictions[41] and the experimental results of Zube and Myers.[20]

Numerical Model

The strong coupling of ohmic, diffusive, viscous, and chemical kinetic processes in an arcjet dictates the use of a complex numerical model to predict details of the plasmadynamic flow. At the same time, such models must be validated experimentally to verify the results. A model developed by Megli et al.[40,41] is used here to predict velocity and gas temperature at the exit plane.

The calculations incorporate an axisymmetric, steady, laminar two-temperature kinetic nonequilibrium approach for modeling an arcjet operating on N_2/H_2 mixtures. The model is an axisymmetric, seven-species hydrogen/nitrogen plasma code that solves the computational domain up to the exit plane. Separate energy equations are formulated and solved for the electrons and the heavy species. The tungsten anode temperature distribution is included, and the plasma electrical conductivity is coupled with the plasma properties, which allows a self-consistent solution for the current distribution. The model is capable of both chemical equilibrium and nonequilibrium simulations. A complete discussion of the model and assumptions has been presented elsewhere.[40,41]

In Figs. 10–12, comparisons are made between experimental results and model predictions for the 1-kW arcjet at 50 mg/s of simulated hydrazine propellant. The arc current is 10.0 A for both model and experiment, and a chemical nonequilibrium simulation is employed.[41] Figure 10 compares the predicted axial velocity profile from the model and the results of the TOF probe surveys. Agreement is excellent and within experimental error near the axis. The numerically predicted profile is slightly narrower and more peaked than the measured profile. This is an expected result because the model flow expansion is constrained by the nozzle, which differs from the unconstrained expansion that occurs in the plume in the vicinity of the TOF probe.

Figure 11 displays the probe-derived radial profile of heavy-particle temperature in comparison with the numerical model for $r < 3$ mm. Agreement is excellent for $r < 2$ mm and is not good at $r = 3$ mm, probably because of probe misalignment with the flow.

Figure 12 shows the results of N_2 vibrational and rotational temperature measurements performed by Zube and Myers[20] in the nozzle of an identical thruster at $I_{arc} = 9$ A and $\dot{m} = 47.6$ mg/s, together with the value of T_g determined in the present study and the model heavy particle temperature prediction. The centerline exit plane heavy particle temperature model predictions agree favorably with this experiment ($T_{g,model} = 2800$ K, $T_{g,exp} = 3000$ K) and with the results of Zube and Myers.[20]

Summary and Conclusions

A spatially resolved TOF electrostatic probe technique for measuring plasma axial velocity has been developed and implemented in the very near-field plume of a 1-kW hydrazine arcjet. A radial profile of axial velocity measured at the exit plane has a peak centerline velocity of 6500 m/s at $P/\dot{m} = 22$ MJ/kg, consistent with the known thruster specific impulse. Comparison with previous quadruple probe results for the ion speed ratio u_i/c_m yields $T_g = T_i = 3000$ K at the thruster exit plane, and the degree of thermal nonequilibrium is quantified as $T_g/T_e \sim 0.4$. The measured radial profile of T_g is also symmetric.

The velocity and gas temperature results are compared with previous experimental results and with the predictions of a numerical H_2/N_2 arcjet model. Agreement with the model is favorable for both the exit plane centerline T_g and radial T_g and u_i profiles.

Acknowledgments

The authors acknowledge equipment support by the NASA Lewis Research Center. This work is funded by the Air Force Office of Scientific Research under contracts F49620-92-J-0448 and -0280. Mitat Birkan was the Program Manager. The authors also acknowledge T. W. Megli for supplying the arcjet computational model results. We thank N. T. Tiliakos and G. F. Willmes for their helpful discussions, J. A. Hamley of NASA Lewis Research Center for his very helpful guidance regarding the time-of-flight current pulse circuitry, and M. J. Kushner and J. Mazumder for helpful suggestions.

References

[1]Wilbur, P. J., Jahn, R. G., and Curran, F. C., "Space Electric Propulsion Plasmas," *IEEE Transactions on Plasma Science*, Vol. 19, No. 6, 1991, pp. 1167–1179.

[2]Curran, F. M., and Haag, T. W., "Extended Life and Performance Test of a Low-Power Arcjet," *Journal of Spacecraft and Rockets*, Vol. 29, No. 4, 1992, pp. 444–452.

[3]Bufton, S. A., "Exit Plane Plasma Measurements of a Low-Power Hydrazine Arcjet," Ph.D. Dissertation, Univ. of Illinois at Urbana–Champaign, IL, 1995.

[4]Langmuir, I., and Mott-Smith, H. M., "The Theory of Collectors in Gaseous Discharges," *Physical Review*, Vol. 28, 1926, pp. 727–763.

[5]Carney, L. M., and Keith, T. G., "Langmuir Probe Measurements of an Arcjet Exhaust," *Journal of Propulsion and Power*, Vol. 5, No. 3, 1989, pp. 287–294.

[6]Carney, L. M., and Sankovic, J. M., "The Effects of Arcjet Operating Condition and Constrictor Geometry on the Plasma Plume," AIAA Paper 89-2723, July 1989.

[7]Sankovic, J. M., "Investigation of the Arcjet Plume Near Field Using Electrostatic Probes," NASA TM-103638, Nov. 1990.

[8]Sankovic, J., and Jankovsky, R., "An Experimental Investigation of the Effective Current Collecting Area of a Spherical Langmuir Probe in an Arcjet Thruster Exhaust," AIAA Paper 90-0073, Jan. 1990.

[9]Gallimore, A. D., Kim, S.-W., Foster, J. E., King, L. B., and Gulczinski, F. S., "Near and Far-Field Plume Studies of a 1 kW Arcjet," AIAA Paper 94-3137, June 1994.

[10]Chen, S.-L., and Sekiguchi, T., "Instantaneous Direct-Display System of Plasma Parameters by Means of Triple Probe," *Journal of Applied Physics*, Vol. 36, No. 8, 1965, pp. 2363–2375.

[11]Tilley, D. L., Kelly, A. J., and Jahn, R. G., "The Application of the Triple Probe Method to MPD Thruster Plumes," AIAA Paper 90-2667, July 1990.

[12]Tilley, D. L., Gallimore, A. D., Kelly, A. J., and Jahn, R. G., "The Adverse Effect of Perpendicular Ion Drift Flow on Cylindrical Triple Probe Electron Temperature Measurements," *Review of Scientific Instruments*, Vol. 65, No. 3, 1994, pp. 678–681.

[13]Burton, R. L., DelMedico, S. G., and Andrews, J. C., "Application of a Quadruple Probe Technique to MPD Thruster Plume Measurements," *Journal of Propulsion and Power*, Vol. 9, No. 5, 1993, pp. 771–777.

[14]Burton, R. L., and Bufton, S. A., "Exit-Plane Electrostatic Probe Measurements of a Low-Power Arcjet," *Journal of Propulsion and Power*, Vol. 12, No. 6, 1996, pp. 1099–1106.

[15]Kanal, M., "Theory of Current Collection of Moving Cylindrical Probes," *Journal of Applied Physics*, Vol. 35, No. 6, 1964, pp. 1697–1703.

[16]Bruce, C., and Talbot, L., "Cylindrical Electrostatic Probes at Angles of Incidence," *AIAA Journal*, Vol. 13, No. 9, 1975, pp. 1236–1238.

[17]Johnson, B. H., and Murphree, D. L., "Plasma Velocity Determination by Electrostatic Probes," *AIAA Journal*, Vol. 7, No. 10, 1969, pp. 2028–2030.

[18]Poissant, G., and Dudeck, M., "Velocity Profiles in a Rarefied Argon Plasma Stream by Crossed Electrostatic Probes," *Journal of Applied Physics*, Vol. 58, No. 5, 1985, pp. 1772–1779.

[19]Tiliakos, N. T., Burton, R. L., and Krier, H., "Application of Internal Langmuir Diagnostics for Arcjets," AIAA Paper 95-2386, July 1995.

[20]Zube, D. M., and Myers, R. M., "Thermal Nonequilibrium in a Low-Power Arcjet Nozzle," *Journal of Propulsion and Power*, Vol. 9, No. 4, 1993, pp. 545–552.

[21]Hargus, W., Micci, M., and Spores, R., "Interior Spectroscopic Investigation of the Propellant Energy Modes in an Arcjet Nozzle," AIAA Paper 94-3302, June 1994.

[22]Zube, D. M., and Auweter-Kurtz, M., "Spectroscopic Arcjet Diagnostic Under Thermal Equilibrium and Nonequilibrium Conditions," AIAA Paper 93-1792, June 1993.

[23]Zube, D. M., and Messerschmid, E. W., "Spectroscopic Temperature and Density Measurements in a Low Power Arcjet Plume," AIAA Paper 94-2744, June 1994.

[24]Habiger, H. A., Auweter-Kurtz, M. and Kurtz, H., "Investigation of Arc Jet Plumes with Fabry-Perot Interferometry," AIAA Paper 94-3300, June 1994.

[25]Golz, T. M., Auweter-Kurtz, M., Habiger, H., and Kurtz, H. L., "High Specific Impulse Performance of a 100 kW Radiation Cooled Thermal Arcjet Thruster," AIAA Paper 94-3249, June 1994.

[26]Pivirotto, T. J., "Velocity and Atom Temperature Distribution Measurement in Arcjet Engine Plumes," *Proceedings for the Arcjet Plume Diagnostics Technical Workshop* (Pasadena, CA), 1986, pp. 179–190.

[27]Irwin, D. A., Pham-Van-Diep, G. C., and Deininger, W. D., "Laser-Induced Fluorescence Measurements of Flow Velocity in High-Power Arcjet Thruster Plumes," *AIAA Journal*, Vol. 29, No. 8, 1991, pp. 1298–1303.

[28]Burtner, D., Keefer, D., and Ruyten, W., "Experimental and Numerical Studies of a Low-Power Arcjet Operated on Simulated Ammonia," AIAA Paper 94-2869, June 1994.

[29]Liebeskind, J. G., Hanson, R. K., and Cappelli, M. A., "Experimental Investigation of Velocity Slip near an Arcjet Exit Plane," *AIAA Journal*, Vol. 33, No. 2, 1995, pp. 373–375.

[30]Liebeskind, J. G., Hanson, R. K., and Cappelli, M. A., "Flow Diagnostics of an Arcjet Using Laser-Induced Fluorescence," AIAA Paper 92-3243, July 1992.

[31]Pobst, J. A., Wysong, I. J., and Spores, R. A., "Laser Induced Fluorescence of Ground State Hydrogen Atoms at the Nozzle Exit of an Arcjet Thruster," AIAA Paper 95-1973, June 1995.

[32]Storm, P. V., and Cappelli, M. A., "Laser-Induced Fluorescence Measurements Within an Arcjet Thruster Nozzle," AIAA Paper 95-2381, June 1995.

[33]Storm, P. V., and Cappelli, M. A., "Axial Emission Measurements on a Medium Power Hydrogen Arcjet Thruster," AIAA Paper 94-2743, June 1994.

[34]Pobst, J. A., Schilling, J. H., Erwin, D. A., and Spores, R. A., "Time Resolved Measurements of 1 kW Arcjet Plumes Using Current Modulation Velocimetry and Triple Langmuir Probes," International Electric Propulsion Conf., Paper 93-128, Sept. 1993.

[35]Pobst, J. A., Schilling, J. H., Lutfy, F. M., Erwin, D. A., and Spores, R. A., "Arcjet Diagnostics Using Current Modulation Velocimetry and Pulsed Electron Beam Fluorescence," AIAA Paper 94-2742, June 1994.

[36]Spores, R. A., Pobst, J. A., Schilling, J. H., and Erwin, D. A., "Performance Effects of Interaction Between a Low-Power Arcjet and Its Power Processing Unit," AIAA Paper 92-3238, July 1992.

[37]Hoell, J. M., Burlock, J., and Jarrett, O., "Velocity and Thrust Measurements in a Quasi-Steady Magnetoplasmadynamic Thruster," *AIAA Journal*, Vol. 9, No. 10, 1971, pp. 1969–1974.

[38]Habiger, H. A., Auweter-Kurtz, M., and Kurtz, H., "Electrostatic Probes for the Investigation of Arc-Driven Electric Propulsion Devices," *Proceedings of the 23rd International Electric Propulsion Conference*, Seattle, WA, 1993, pp. 1137–1147.

[39]Burton, R. L., Bufton, S. A., Tiliakos, N. T., and Krier, H., "Application of Multiple Electrostatic Probes to a Low Power Arcjet," AIAA Paper 94-3299, June 1994.

[40]Megli, T. W., Krier, H., Burton, R. L., and Mertogul, A., "Two-Temperature Modeling of N_2/H_2 Arcjets," AIAA Paper 94-2413, June 1994.

[41]Megli, T. W., Krier, H., and Burton, R. L., "A Plasmadynamics Model for Nonequilibrium Processes in N_2/H_2 Arcjets," AIAA Paper 95-1961, June 1995.